Int. J. Radiation Oncology Biol. Phys., Vol. 63, No. 3, pp. 921–929, 2005

0360-3016/05/$–see front matter

ELSEVIER

doi:10.1016/j.ijrobp.2005.03.070

PHYSICS CONTRIBUTION

NOVEL BREATHING MOTION MODEL FOR RADIOTHERAPY

DANIEL A. LOW, PH.D.,* PARAG J. PARIKH, M.D.,* WEI LU, PH.D.,* JAMES F. DEMPSEY, PH.D.,†
SASHA H. WAHAB, M.D.,* JAMES P. HUBENSCHMIDT, B.S.,*
MICHELLE M. NYSTROM, B.S.,* MAUREEN HANDOKO, B.S.,* AND JEFFREY D. BRADLEY, M.D.*

*Department of Radiation Oncology, Washington University School of Medicine, St. Louis, MO; †Department of Radiation Oncology, University of Florida, Gainesville, FL

Purpose: An accurate model of breathing motion under quiet respiration is desirable to obtain the most accurate and conformal dose distributions for mobile lung cancer lesions. On the basis of recent lung motion measurements and the physiologic functioning of the lungs, we have determined that the motion of lung and lung tumor tissues can be modeled as a function of five degrees of freedom, the position of the tissues at a user-specified reference breathing phase, tidal volume and its temporal derivative airflow (tidal volume phase space). Time is an implicit variable in this model.

Methods and Materials: To test this hypothesis, a mathematical model of motion was developed that described the motion of objects p in the lungs as linear functions of tidal volume and airflow. The position of an object was described relative to its position $\vec{P}_0$ at the reference tidal volume and zero airflow, and the motion of the object was referenced to this position. Hysteresis behavior was hypothesized to be caused by pressure imbalances in the lung during breathing and was, in this model, a function of airflow. The motion was modeled as independent tidal volume and airflow displacement vectors, with the position of the object at time t equal to the vector sum $\vec{r}_P(t) = \vec{r}_v(t) + \vec{r}_f(t)$ where $\vec{r}_v(t)$ and $\vec{r}_f(t)$ were displacement vectors with magnitudes approximated by linear functions of the tidal volume and airflow. To test this model, we analyzed five-dimensional CT scans (CT scans acquired with simultaneous real-time monitoring of the tidal volume) of 4 patients. The scans were acquired throughout the lungs, but the trajectories were analyzed in the couch positions near the diaphragm. A template-matching algorithm was implemented to identify the positions of the points throughout the 15 scans. In total, 76 points throughout the 4 patients were tracked. The lateral motion of these points was minimal; thus, the model was described in two spatial dimensions, with a total of six parameters necessary to describe the 30 degrees of freedom inherent in the 15 positions.

Results: For the 76 evaluated points, the average discrepancy (the distance between the measured and prediction positions) of the 15 locations for each tracked point was 0.75 ± 0.25 mm, with an average maximal discrepancy of 1.55 ± 0.54 mm. The average discrepancy was also tabulated as a fraction of the breathing motion. Discrepancies of <10% and 15% of the overall motion occurred in 73% and 95% of the tracked points, respectively.

Conclusion: The motion tracking algorithms are being improved and automated to provide more motion data to test the models. This may allow a measurement of the motion-fitting parameters throughout the lungs. If the parameters vary smoothly, interpolation may be possible, yielding a continuous mathematical model of the breathing motion throughout the lungs. The utility of the model will depend on its stability as a function of time. If the model is only robust during the measurement session, it may be useful for determining lung function. If it is robust for weeks, it may be useful for treatment planning and gating of lung treatments. The use of tidal volume phase space for characterizing breathing motion appears to have provided, for the first time, the potential for a patient-specific mathematical model of breathing motion. © 2005 Elsevier Inc.

Radiotherapy, Breathing motion, five-dimensional CT, Lung motion.

INTRODUCTION

The introduction of multislice CT scanners has led to development of processes to measure the breathing motion of tumors for radiotherapy planning (1, 2). Various techniques for measuring or controlling breathing motion have been proposed, all aimed at concentrating a prescribed dose to the tumor and minimizing radiation to surrounding normal tissue. These techniques include fluoroscopic imaging of the tumor motion (3), tracking internal markers (4–6), monitoring external markers (7–9), breath holding (10–12) or active breathing control (13), and using a spirometer to monitor lung tidal volume changes (1, 14–17).

Breathing motion has, by most groups, been modeled as a function of the breathing phase. Vedam *et al.* (7) characterized breathing as a cyclic process and subdivided breath-

Reprint requests to: Daniel A. Low, Ph.D., Department of Radiation Oncology, Washington University School of Medicine, 4921 Parkview Pl., St. Louis, MO 63110. Tel: (314) 362-2636; Fax: (314) 362-8521; E-mail: low@wustl.edu

Received Nov 11, 2004, and in revised form Mar 25, 2005. Accepted for publication Mar 28, 2005.

ing into eight phases: peak exhalation, early, mid, and late inhalation, peak inhalation, and early mid and late exhalation. The authors applied this phase model to binning CT scans as a function of the breathing phase. Although the strategy was robust for a mechanical phantom and regular breathing cycles, the phase definitions broke down with irregular breathing. Lujan *et al.* (18) described diaphragm motion using a periodic, but asymmetric, function that had a constant period.

One reason for the attraction of the phase-based description of breathing has been that many objects in the lung do not move along the same path during inhalation and exhalation. This was observed by Seppenwoolde *et al.* (5) during fluoroscopic-based monitoring of radiopaque clips using equipment and techniques described by Shirato *et al.* (4, 19). Seppenwoolde *et al.* (5) showed examples of the trajectories of clips placed in 21 tumors, many of which exhibited this hysteresis-like behavior. Seppenwoolde *et al.* (5) provided a mathematical description of this motion by showing two idealized tracks, with the motion along each coordinate modeled as an even power of a cosine function in time. The relative phase difference between the cosine functions determined the amount of hysteresis. Although they did not claim that they were presenting a mathematical model of breathing, the point of the discussion was that breathing motion could be modeled as a function of time. One of the difficulties with this approach was shown in their report, in which they modeled the breathing motion using the cosine functions, but the parameters of the fit could not be predicted as a function of time. Neicu *et al.* (20), in defining a process that directly measured radiopaque markers placed within the lungs, defined regular and irregular breathing cycles for which their gating technique would and would not be accurate.

Manke *et al.* (21) described a breathing motion model for coronary magnetic resonance angiography that used a patient-adapted affine model. They used diaphragm position as the breathing surrogate. They compared hysteresis motion modeling with a single diaphragmatic navigator, three navigators, and a single diaphragmatic navigator and a precursory navigator, which was a phase-shifted navigator (200 ms). The precursory navigator provided sensitivity to the change in the diaphragm position and was an approximation of the diaphragm velocity, providing the sensitivity the respiratory phase needed to model hysteresis motion. As such, their report provided an initial attempt to correlate the rate of the surrogate motion (diaphragm motion) to hysteresis and appeared to be quite successful.

We hypothesized that purely phase-based models would be fundamentally inappropriate to characterize breathing motion due to quiet, uncoached respiration. Although breathing is a periodic function when seen as a function of time, neither the amplitude nor frequency of uncoached breathing can be predicted as a function of time. Even when monitoring breathing, purely phase-based approaches, in which the motion amplitude is described by the phase of breathing, do not adequately model variations from breath to breath.

We have developed our CT scanning protocols used to measure breathing motion using real-time tidal volume measurements as the surrogate by which we have gated the CT data (22–24). The motion of each object within the lung was characterized by the three-dimensional position of the object at a reference breathing phase, for example at tidal exhalation. Because quiet respiration was not perfectly regular, we defined the breathing phases using a statistical definition of tidal volume based on a percentile system. The percentile tidal volume v_c was defined as the tidal volume for which the patient had that tidal volume or less, c percent of the time. For example, v_5 indicated the tidal volume for which the patient had in the lungs that amount or less of air only 5% of the time during the scanning session. We typically selected v_5 to define exhalation, although different values were selected for very irregular breathing cycles. However, tidal volume alone did not, in itself, suffice for modeling the breathing motion because modeling hysteresis was not possible if the breathing phase was not considered as well. In the absence of a more complete solution, we subdivided breathing into inhalation and exhalation to allow a crude characterization of hysteresis (22).

The action of inhalation involves the body's creation of a vacuum in the lungs by tension in the diaphragm and chest wall. The greater the vacuum created, the greater the airflow into the lungs. To the first order, the rate of airflow will be proportional to the vacuum created. It has been known for some time (25, 26) that pressure disequilibria exist throughout the lungs during breathing caused by differential airflow resistance to these regions. In general, during inhalation, regions that have better and worse communication with air in the trachea will have greater and lesser air pressure during inhalation, respectively, with the opposite during exhalation. If the hysteresis is caused by these pressure disequilibria, it is logical to assume that the effects of hysteresis, namely the differential motion between inhalation and exhalation, can be characterized as a function of airflow, defined as the time derivative of the tidal volume.

Therefore, we hypothesized that breathing motion can be parameterized as a function of five dimensions (5D). The position of an object in the lungs was parameterized by its 3D position at the reference breathing phase. The position of the object at time t is a function of tidal volume $v(t)$ and airflow $f(t)$ (tidal volume phase space). The process of acquiring CT data during simultaneous tidal volume measurements for purposes of mapping or characterizing breathing motion was termed 5D CT, in which time was considered only implicitly.

METHODS AND MATERIALS

Model

The dependence of breathing motion on these five dimensions was insufficient to characterize quantitatively the motion in a patient; a mathematical model was also required. As a first step, we developed a linear motion model to test our 5D hypothesis in which the motion due to the tidal volume and airflow (hysteresis) was separated. The motion model of an object in the lung is

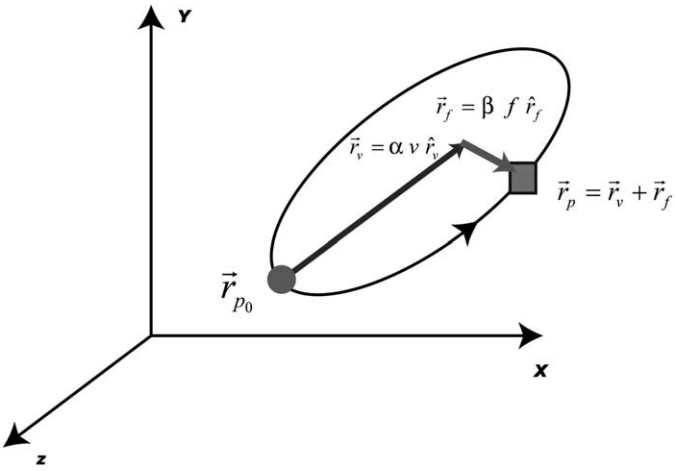

Fig. 1. Mathematical characterization of motion of object (shown as circle in reference breathing phase at $\vec{r}_{P_0}$ and square at arbitrary phase at point $\vec{r}_P$) in lungs. Tidal volume and airflow indicated by v and f, respectively. $\boldsymbol{r}_v$ and $\boldsymbol{r}_f$ vector is tidal volume and airflow displacement vector, respectively.

summarized in Fig. 1. The object is shown as a circular dot at the reference breathing phase, selected in this example to be at tidal exhalation, at position $\vec{r}_{P_0}$. The object moves owing to the tidal volume and airflow to position $\vec{r}_P$ relative to $\vec{r}_{P_0}$. The displacement vector $\vec{r}_P$ is separated into two independent displacement vectors that are independent functions of tidal volume and airflow, $\vec{r}_v$ and $\vec{r}_f$, $\vec{r}_v$ and $\vec{r}_f$ is termed the tidal volume and airflow vector with a unit vector of $\hat{r}_v$ and $\hat{r}_f$, respectively. The linear model further described $\boldsymbol{r}_v$ and $\boldsymbol{r}_f$ by the constants α and β multiplied by the scalar tidal volume v and airflow f value, respectively:

$$\boldsymbol{r}_v = \alpha\ v\ \hat{r}_v \tag{1}$$

and

$$\boldsymbol{r}_f = \beta f\ \hat{r}_f \tag{2}$$

where $\hat{r}_v$ and $\hat{r}_f$ are the unit vectors along the tidal volume and airflow axes, indicating the direction of motion of the object due to tidal volume and airflow variations, respectively. The quantities α, β, $\hat{r}_v$ and $\hat{r}_f$ are functions of $\vec{r}_{P_0}$; that is, they vary throughout the lungs and their values are determined by using patient image data.

Validation image data set acquisition

This model was tested on 4 patient CT data sets acquired using our newly labeled 5D-CT technique (22–24). Fifteen CT scans were acquired using a 16-slice CT scanner (Sensation 16, Siemens Medical Systems, Concord, CA) operating in 12-slice mode with 1.5-mm-thick slices (18-mm total scanned thickness). The scanner was operated in cine mode using a 0.5-s rotation, 360° reconstruction, and 0.25 s between CT scans, requiring 11 s to acquire the 15 scans. Each 18-mm-thick region was termed the "couch position," and 14–17 couch positions were typically required to scan the entire lungs of a patient.

Quantitative spirometry-measured tidal volume was simultaneously acquired (22–24). The tidal volume was measured using a calibrated digital spirometer (VMM 400, Interface Associates, Laguna Niguel, CA) that was sampled at 100 Hz and had a 1-mL digitization resolution. The digitization resolution was sufficiently coarse that a simple differentiation of the tidal volume curve yielded unacceptable artifacts in the airflow curve. Therefore, the tidal volume derivative was approximated at a time t by fitting the tidal volume curve throughout the range $t \pm 0.2$ s (41 points) to a fifth-order polynomial and taking the analytic derivative. Examination of the tidal volume data and resulting fit showed excellent correspondence. Even with this approach, the airflow curves contained residual digitization artifacts of approximately 10% of the maximal flow rates.

Our group has been active in the quantitative measurement and evaluation of breathing motion (1, 22, 23, 27–30). We previously evaluated the accuracy and precision of our 5D-CT techniques by comparing tidal volume to air content, defined as the amount of air in the lungs, bronchi, and trachea subtended by a single couch position. The relationship between the air content and tidal volume was remarkably linear, even for couch positions that subtended the diaphragm. Owing to differences in air density in the lungs vs. in the CT scanning room, air entering the lungs expanded by a factor of 1.11. Therefore, the rate of air content change summed throughout all couch positions that intercepted lung should have been 1.11 times the airflow as measured by spirometry. For 12 patients, the measured value was 1.08 ± 0.06, indicating that the 4D-CT process yielded accurate reconstructions (22). The standard deviation of a linear fit between the air content and tidal volume was assumed to provide an upper bound on the measurement-to-measurement precision of the 4D-CT process. For all patients, the precision was 8% or better relative to the total tidal volume, with a mean value of $5.1\% \pm 1.9\%$. The good correlation between air content and tidal volume was due in part to the lack of detectable hysteresis in the air content data. Had significant hysteresis been present in the air content, such as has been reported for internal object motion, the correlation would have suffered.

Breathing motion measurements and model fits

We tested our model (Eqs. 1 and 2 and Fig. 1) using trajectories tracked using the 5D-CT data. The CT data were first converted into air content images by techniques described by Lu *et al.* (22) These resulted in 3D images whose voxel values were equal to the fraction of air content in those voxels. The images were ranked in order of tidal volume, first for scans acquired during inhalation and then exhalation. These scans were often acquired during several breaths. Trajectories were obtained for selected regions in the air content images by first defining a template with the location of the template selected manually using 1 of the 15 image sets (the 1 nearest mid-exhalation). The criterion for selection was that the template contain a high-contrast object near its center (e.g., bronchial branch points). For the CT image data sets, the voxels extended 0.938 mm in the lateral and AP directions. The templates size was $20 \times 20 \times 8$ voxels, corresponding to $18.75 \times 18.75 \times 12$ mm^3. The location of the same tissues in subsequent images was determined by computing the normalized correlation coefficient between the template and regions of the same size in the subsequent image. A search was conducted to find the peak value of the correlation. Although only translations of the template were allowed, the purpose of the template-matching process was to determine the motion of the template center. The registration results were checked visually to verify the template-matching process. This process was repeated for the 14 images to provide 15 sets of (x, y, z) locations. In addition, the tidal volume and airflow were known for each of the 15 positions. Given the relatively coarse CT voxel spacing, the templates were positioned in couch positions near the

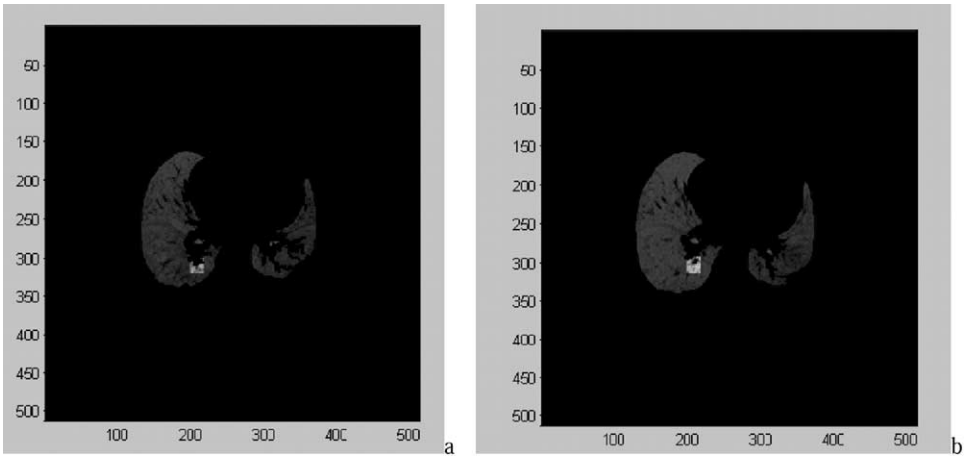

Fig. 2. Template example used to track lung objects for validation of motion model. Near tidal volume (a) exhalation and (b) inhalation.

diaphragm to provide relatively large motions. The accuracy of the template matching was assumed to be within one voxel.

For the templates studied, lateral motion was negligible; thus, a 2D representation of Eqs. 1 and 2 was used to model the motion. The measured data were fit to the model by minimizing the root-mean least-squares average distance between the fits and measurements. Because of the voxel size, the accuracy of the trajectory mapping was estimated as one-half the voxel size, or 0.5 mm and 0.75 mm in the AP and craniocaudal direction, respectively. The spatial discrepancies between the fit and measured positions were tabulated as metrics of the fit accuracy. For the 2D motion, there were six fitting parameters (α, β, $\hat{r}_v$ and $\hat{r}_f$, and the two spatial components of $\vec{r}_{P_0}$ and 30 degrees of freedom (two displacements in each of the 15 images). In the following results, the two axes corresponded to the craniocaudal and AP directions, with increasing values in the superior and posterior direction, respectively.

RESULTS

Figure 2 shows an example of the template matching technique for Patient 1. Transverse air content images are shown, and the template region from the first scan is highlighted. Figure 2a shows the template scan (lowest tidal volume during inhalation) and Fig. 2b shows the maximal tidal volume. The correspondence was evident despite the large variations in tidal volume.

Figures 3 and 4 show an example of the model fits for two templates in different couch positions for Patient 1. Figure 4a shows the tidal volume distribution for the 11-s period of the scan, with crosses indicating the times the scans were acquired. For each case, the measured data included multiple breaths. This is a significant advantage of using the cine, rather than the helical, CT acquisition mode, because the amount of time over which the scans are acquired is not limited by the minimum couch translation speed. Figure 4b shows the measured (crosses) and fit (circles) positions of the tracked templates. Lines connecting the corresponding measured and fit points were provided as aid to the eye, and the axis origins have been placed at the location of $\vec{r}_{P_0}$ for the template being evaluated. To provide a quantitative review of the fit quality, Fig. 4c shows histograms of the discrepancies. Because the continuous tidal volume curves were available, the model allowed a prediction of the continuous motion of the templates throughout the scan session. The model predictions of the continuous motion of the template are shown in Figs. 3d and 4b. The motion due entirely to the tidal volume vector is shown as a line emerging from $\vec{r}_{P_0}$. Triangles were drawn along the lines to indicate the predicted template positions at 100-mL intervals.

Some important features of this technique can be seen in the images shown in Figs. 3 and 4. First, the breathing patterns were not regular, and the patients had not been coached during the scanning sessions. The only instructions given were to remain as still as possible, except for breathing. None of the more than 35 patients scanned to date was unable to understand and attempt to follow this request. In 2 cases, the patients were unable to remain still enough to complete the CT scans, because they could not lay down for more than a couple of minutes. For Figs. 3 and 4, the fits were remarkably good, with average discrepancies of 0.5 mm and maximal discrepancies $<$1 mm, of a total motion range of 6–11 mm. This indicated that the model worked extremely well for the 11-s periods representative of the scanning sessions.

The breathing pattern shown in Fig. 4 had some remarkable features. At the beginning of the scan, the patient underwent a breath of only 70 mL, very small compared with a normal tidal volume of 500 mL. The subsequent three breaths were more even, but the inhalation and exhalation volume still varied by $>$100 and 50 mL, respectively. Despite the wide tidal volume variation, the linear motion model still did extremely well, with an average and maximal discrepancy of 0.5 and 0.9 mm, respectively. Coincidentally, a CT scan was acquired near the peak of the small breath and the peaks of the next two normal breaths (68, 488, and 414 mL). For the 19 tracked points and each of these breath peaks, the predicted and measured positions agreed within 1.12 $\pm$ 0.41 mm, 0.80 $\pm$ 0.76 mm, 0.66 $\pm$ 0.40 mm of an average total motion of 10.3 mm from inhalation to exhalation. This agreement was excellent,

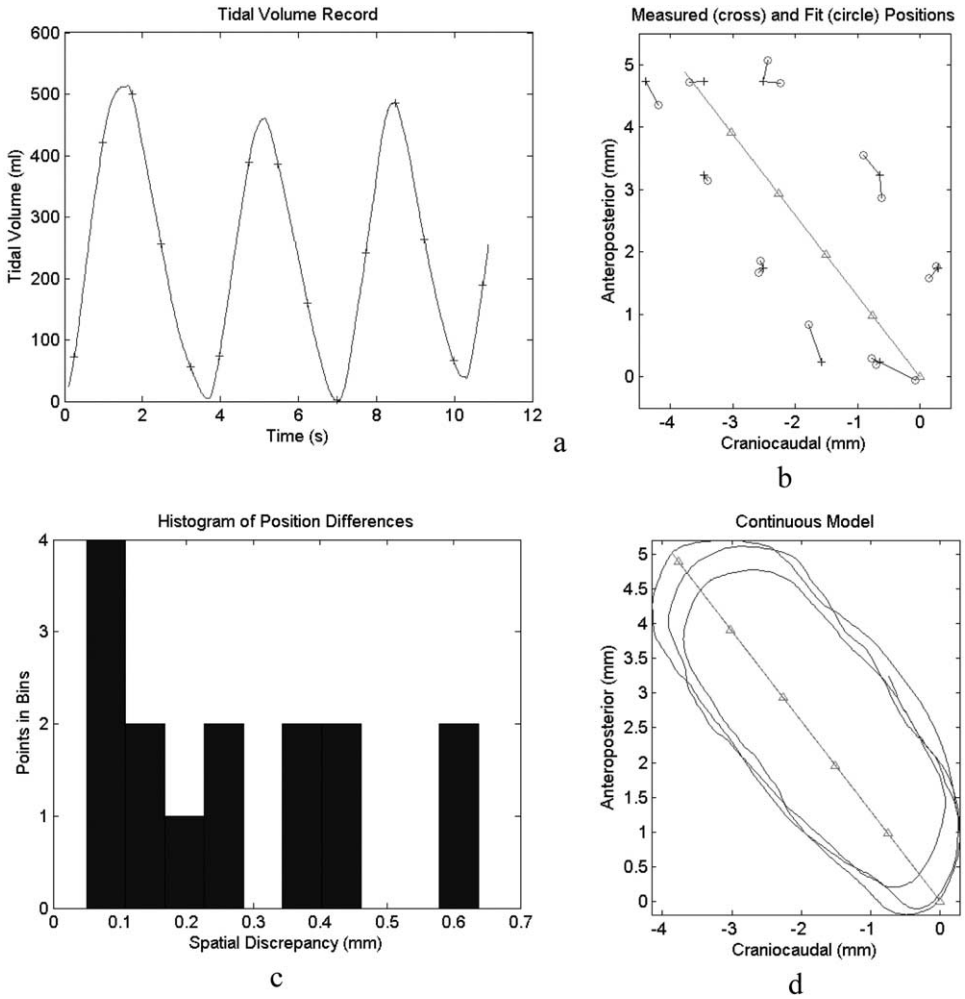

Fig. 3. Example of 5D motion model results for Patient 1, couch position 10. Breathing pattern during CT acquisition at this couch position was relatively regular. (a) Tidal volume distribution during 11-s period of CT image acquisition. Crosses indicate times CT scans were acquired. (b) Measured (crosses) and fit (circles) locations of object tracked in 15 CT scans. Because of finite pixel resolution, some measured positions overlapped. Line segments indicate discrepancies between measurements and fits. Line passing through distribution represents zero-flow trajectory, with triangles at intervals corresponding to 100-mL tidal volume (0 mL corresponded to origin on Fig. 3). (c) Histogram of spatial discrepancies showing that, for this case, maximal discrepancy was 0.6 mm. (d) Application of model parameters to continuous tidal volume and airflow distributions measured during CT scan session for this tracked point. Line passing through distribution represents zero-flow trajectory, with triangles at intervals corresponding to 100-mL tidal volume (0 mL corresponded to origin on Fig. 3).

given a factor of seven difference in the depths of these breaths. Pure phase-based breathing models would have termed each of the four breath peaks as "inhalations" and would have failed to model the motion differences during each breath adequately.

The trajectories of both templates shown in Figs. 3 and 4 are both elliptical and of similar shape. Other tracked templates in the same patient had a wide variety of trajectory shapes. Examples are shown in Fig. 5 and consisted of both wider and narrower elliptical trajectories, as well as trajectories with different orientations. The mean and maximal discrepancies were provided for each trajectory.

The comparison of the measured and fit trajectories is shown in Table 1 for the 4 tested patients. The total number of couch positions and templates tracked in each patient is listed, as are the discrepancies between the measurements and fits. The mean and maximal discrepancies were independently determined for each tracked template (15 points). The average of the mean discrepancies, the average of the maximal discrepancies, and the worst-case maximal discrepancy were tabulated.

Of the 76 tracked points, the mean discrepancies ranged from 0.28 to 1.71 mm (average $\pm$ SD, 0.75 $\pm$ 0.25). The maximal discrepancies were as small as 0.64 mm and as large as 3.31 mm (average $\pm$ SD of maximal discrepancy, 1.55 $\pm$ 0.54).

The values of α ranged from 0.0072 to 0.0466 mm $\times$ mL^{-1}, and the maximal tidal volume ranged from 381 to 857 mL for the 4 patients. Using the α values and the tidal volume, the maximal displacement of the tested points ranged from 6.4 to

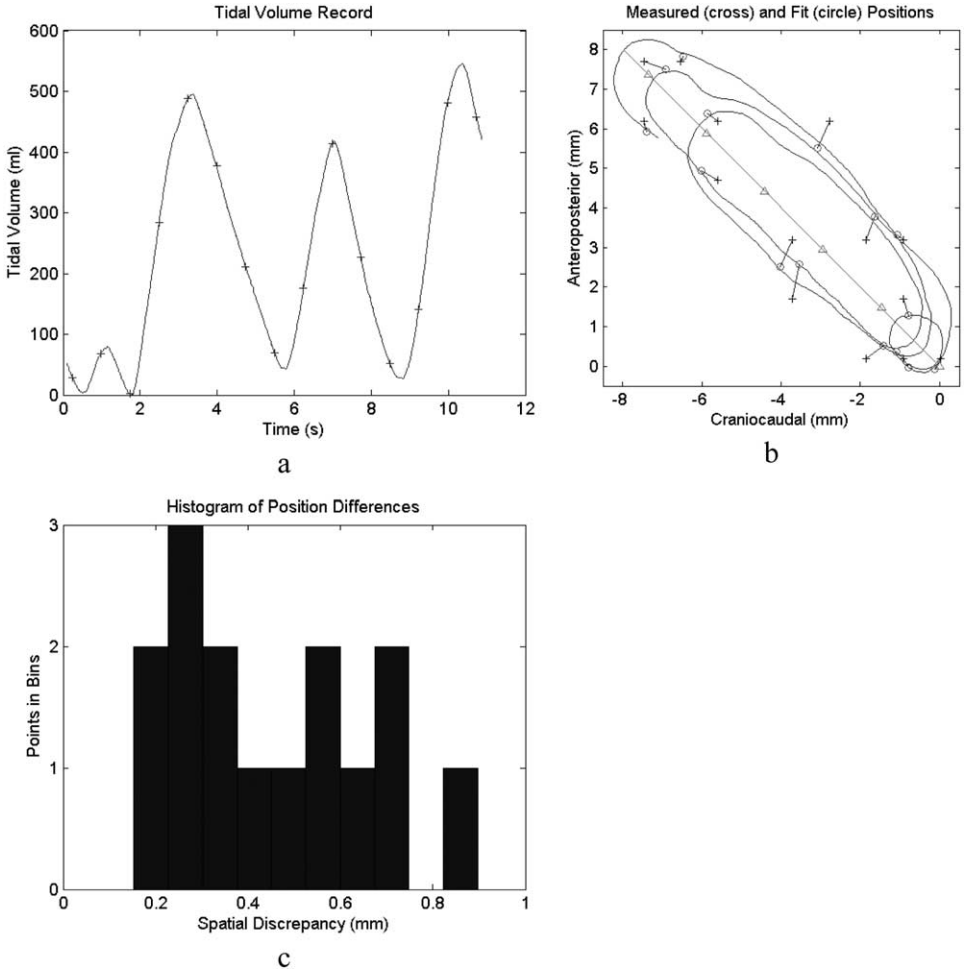

Fig. 4. Example of 5D motion model results for Patient 1, couch position 12. Breathing pattern during CT acquisition at this couch position was irregular. (a) Tidal volume distribution during 11-s period of CT image acquisition. Crosses indicate times CT scans were acquired. (b) Measured (crosses) and fit (circles) locations of object tracked in 15 CT scans. Because of finite pixel resolution, some measured positions overlapped. Lines connecting points indicate discrepancies between measurements and fits. Continuous model prediction of motion also shown. Line passing through distribution represents zero-flow trajectory, with triangles at intervals corresponding to 100-mL tidal volume (0 mL corresponded to origin on Fig. 4). (c) Histogram of spatial discrepancies showing that, for this case, maximal discrepancy was 0.9 mm.

17.5 mm. The mean discrepancy, expressed as a fraction of the maximal displacement, was, therefore <10% for most cases. Figure 6 shows a histogram of the mean discrepancy/maximal displacement ratio for the 76 tracked points. The fraction of the tracked points that had a <10% and <15% average discrepancy was 73% and 95%, respectively, indicating that the model worked extremely well.

The values of α and β are compared in Fig. 7a. α varied from <0.01 mm × mL^{-1} to almost 0.05 mm × mL^{-1}. β varied from almost 0 (no hysteresis) to 0.006 mm × s × mL^{-1}. To better understand the consequences of the numeric values of α and β, the maximal extents due to the tidal volume and airflow vectors were determined by multiplying α and β by the maximal tidal volume and airflow difference (maximal minus minimal airflow), respectively (Fig. 7b, labeled as $|r_f|$ and $|r_v|$. If the displacement due to the airflow and tidal volumes were equal ($|r_f|/|r_v| = 1$), the point would lie along the diagonal line shown in Fig. 7b. The trajectory with the smallest eccentricity had a displacement ratio of $|r_f|/|r_v| = 0.75$, and some of the trajectories were almost straight lines ($|r_f|/|r_v| \approx 0$).

DISCUSSION

The motion of an object in the lung during quiet respiration has been shown to be a function of five degrees of freedom, the location of the object at a user-specified phase of breathing, tidal volume, and airflow (tidal volume phase space). The positions were parameterized by two vectors, tidal volume and airflow. The displacement along these vectors was proportional to the tidal volume and airflow. This model was applied to tracked regions within the lungs of 4 patients, measured using 5D-CT. Despite the relatively simple mathematical model, good agreement between the measured and calculated motion was observed. The average

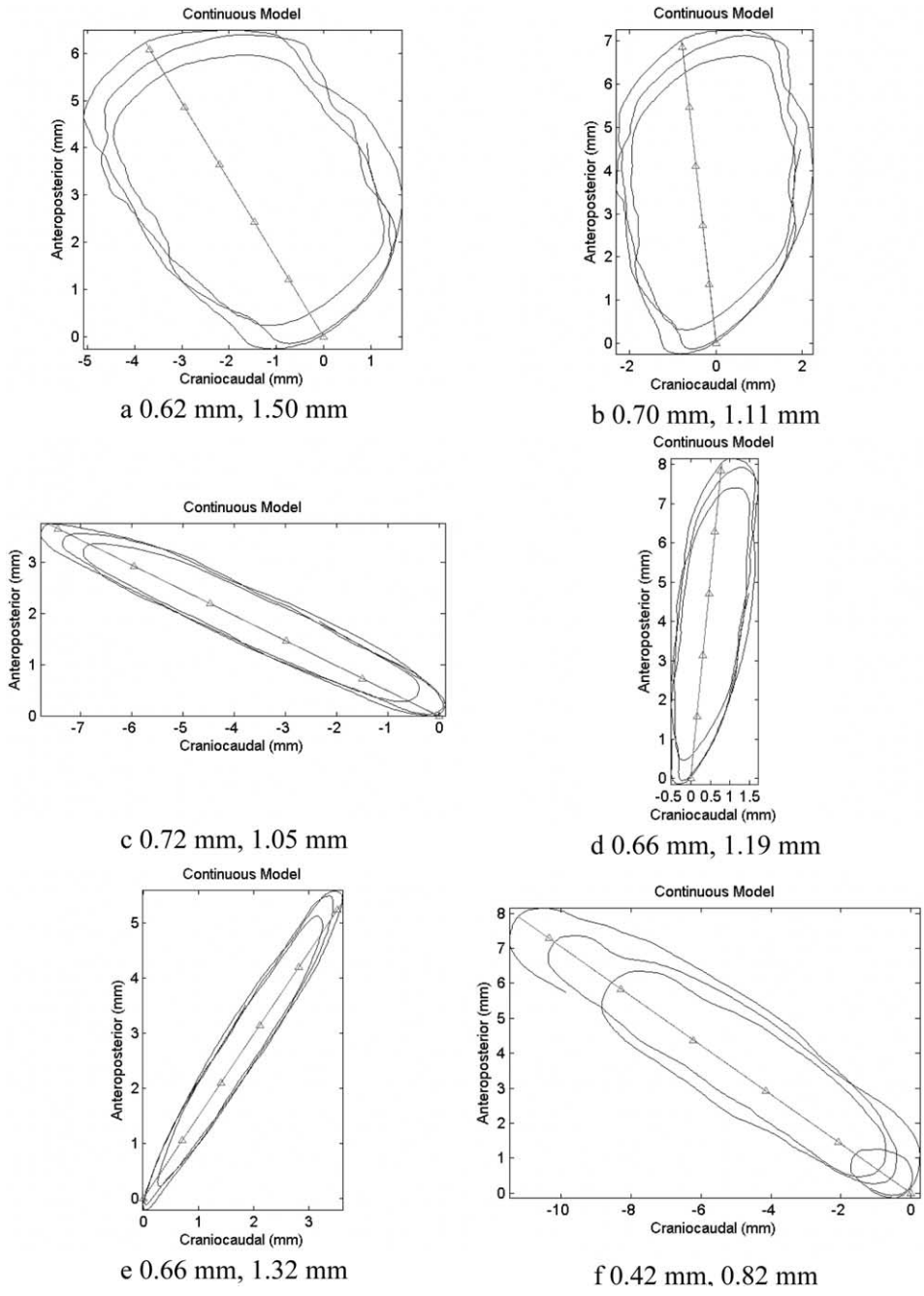

Fig. 5. Examples of continuous motion model predictions of six points within Patient 1. For each location, mean and maximal discrepancies shown. Lines passing through distributions represent zero-flow trajectory, with triangles at intervals corresponding to 100-mL tidal volume (0 mL corresponds to origins in Fig. 5).

discrepancy was better than 15% of the overall motion for 95% of the tracked points.

The points tracked for this study were a small subset of the potential points within the scan data sets. The number that was analyzed was limited by the relatively long time required to select and track each point. We are developing automated techniques for point selection and improving the efficiency of the tracking software to provide a wider array of points, including the tumors, within each patient's lungs. Once this has been completed, we will examine the distribution of fitting parameters to determine whether they vary smoothly across the lungs and can, therefore, be interpolated between measurement points. This will be important in regions of the lungs and tumors in which few distinguishing features are available for tracking. Eventually, the motion model may be used to aid in the deformable registration, acting as a constraint to the motion solution.

For these evaluations, the points were selected in the inferior portions of the lungs where the motion was large, but not so large as to extend beyond a single couch position. Automation of the tracking procedure will make evaluation of the motion in the superior lung more practical. The

Table 1. Summary of breathing motion model fitting of 4 patient cases

Pt. no.	Couch position	Tracked points (n)	Mean discrepancy (mm)	Average maximal discrepancy (mm)	Maximal discrepancy (mm)	Average displacement (mm)
1	10	13	0.61	1.25	1.82	7.4
	11	12	0.68	1.35	2.21	8.4
	12	19	0.68	1.33	1.93	10.3
	14	5	1.07	2.23	3.31	13.2
2	14	1	1.06	2.06	2.06	17.5
3	10	6	1.02	2.18	3.20	13.2
4	10	14	0.78	1.66	2.63	6.4
	12	4	0.81	1.77	1.92	10.2
	13	2	0.90	1.82	1.86	11.0

motion of the inferior portions of the lung extended beyond a single couch position, and the fitting process described here failed when the tracked point exited the couch position. A CT scanner that can acquire 16 slices simultaneously (either 0.75-mm or 1.5-mm thickness, Philips Brilliance, Cleveland OH) has recently been commissioned, and the current imaging protocol acquires 25 CT scans rather than 15. This will increase the range of lung over which the tracked objects remain within a single couch position, although algorithms to track points that cross between couch positions are also being developed.

The linear model was able to predict elliptical-looking trajectories that are consistent with published literature. The nonlinear motion behavior came from the nonlinear time dependence of the tidal volume. The fact that the tidal volume was periodic and that the motion was characterized by the tidal volume and its time-derivative airflow allowed the model to characterize the complex breathing motion.

The motion model may also be predictive. The data examined here showed that the model was accurate for the 11-s period during which the motion data were acquired. The 5D-CT scanning protocols are being repeated both intra- and inter-session to test the time dependence of the model's accuracy. If the model is accurate for a few hours to a few days (to within the accuracy of repositioning the patient), it may be used to predict the internal motion of the tumor and normal organs during breathing if the tidal volume is monitored. If the model is shown to be accurate for a few hours to a few weeks, it may be useful for treatment planning, with or without linear accelerator gating or tumor tracking.

If the model proves to be robust with respect to the patient population and is stable in time, it may prove to be an exciting breakthrough in the characterization of human breathing motion. The modeling of breathing as a function of tidal volume phase space rather than time, coupled with real-time tidal volume measurements, could provide the clinician with an accurate determination of the real-time motion of the tumor

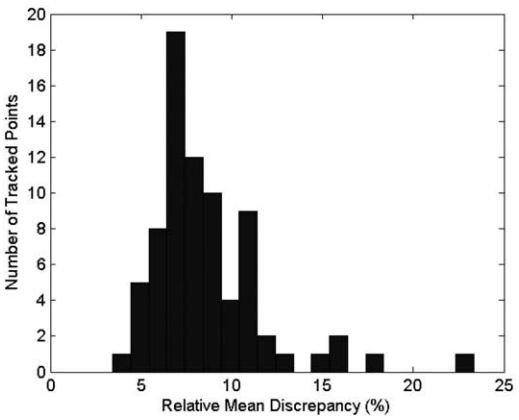

Fig. 6. Histogram of mean discrepancy/point displacement ratio, expressed as percentage, for 76 tracked points.

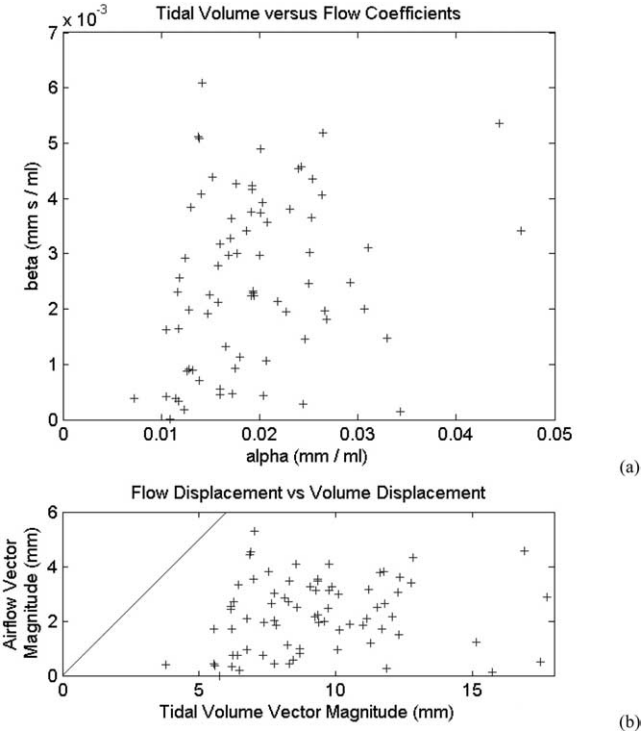

Fig. 7. (a) Comparison between airflow and tidal volume coefficients, α and β. (b) Distances traveled for each point due to airflow and tidal volume variations compared. Line is shown along equal distances, where trajectory would most closely resemble a circle. The smaller the airflow/tidal volume vector magnitude ratio, the greater the eccentricity of the trajectory.

and internal organs during breathing, even for very irregular breathing. Breathing coaching may improve or degrade this relationship because of the unknown effects of conscious self-monitoring and feedback. Additional research is necessary to determine the effects of coaching on breathing motion.

The proposed model does not account for tumor motion due to the cardiac cycle. As the time required to acquire the CT scans decreases (the minimal time with the new CT scanner is currently 0.3 s), tumor motion owing to the cardiac cycle may be imaged in the scans. If the cardiac cycle is measured along with the breathing cycle, it may be possible to add cardiac motion to the model.

The motion model has the potential to map lung function using the measured trajectories. If the model is fundamentally correct in its physical properties, the model parameters should vary smoothly as a function of the position within the lungs. Therefore, interpolation of the model parameters will be possible, and the behavior of the model as a function of position could be used to determine the local filling and emptying by examining the local motion divergence. The motion data should also be able to determine subtle phase differences in the motion of each region, providing additional insights into the lung's function.

REFERENCES

1. Low DA, Nystrom M, Kalinin E, *et al.* A method for the reconstruction of four-dimensional synchronized CT scans acquired during free breathing. *Med Phys* 2003;30:1254–1263.
2. Pan T, Lee TY, Rietzel E, *et al.* 4D-CT imaging of a volume influenced by respiratory motion on multi-slice CT. *Med Phys* 2004;31:333–340.
3. Chen QS, Weinhous MS, Deibel FC, *et al.* Fluoroscopic study of tumor motion due to breathing: Facilitating precise radiation therapy for lung cancer patients. *Med Phys* 2001;28: 1850–1856.
4. Shirato H, Shimizu S, Kitamura K, *et al.* Four-dimensional treatment planning and fluoroscopic real-time tumor tracking radiotherapy for moving tumor. *Int J Radiat Oncol Biol Phys* 2000;48:435–442.
5. Seppenwoolde Y, Shirato H, Kitamura K, *et al.* Precise and real-time measurement of 3D tumor motion in lung due to breathing and heartbeat, measured during radiotherapy. *Int J Radiat Oncol Biol Phys* 2002;53:822–834.
6. Sharp GC, Jiang SB, Shimizu S, *et al.* Prediction of respiratory tumour motion for real-time image-guided radiotherapy. *Phys Med Biol* 2004;49:425–440.
7. Vedam SS, Keall PJ, Kini VR, *et al.* Acquiring a four-dimensional computed tomography dataset using an external respiratory signal. *Phys Med Biol* 2003;48:45–62.
8. Minohara S, Kanai T, Endo M, *et al.* Respiratory gated irradiation system for heavy-ion radiotherapy. *Int J Radiat Oncol Biol Phys* 2000;47:1097–1103.
9. Vedam SS, Keall PJ, Kini VR, *et al.* Determining parameters for respiration-gated radiotherapy. *Med Phys* 2001;28:2139–2146.
10. Hanley J, Debois MM, Mah D, *et al.* Deep inspiration breath-hold technique for lung tumors: The potential value of target immobilization and reduced lung density in dose escalation. *Int J Radiat Oncol Biol Phys* 1999;45:603–611.
11. Rosenzweig KE, Hanley J, Mah D, *et al.* The deep inspiration breath-hold technique in the treatment of inoperable non–small-cell lung cancer. *Int J Radiat Oncol Biol Phys* 2000;48: 81–87.
12. Mah D, Hanley J, Rosenzweig KE, *et al.* Technical aspects of the deep inspiration breath-hold technique in the treatment of thoracic cancer. *Int J Radiat Oncol Biol Phys* 2000;48:1175–1185.
13. Wong JW, Sharpe MB, Jaffray DA, *et al.* The use of active breathing control (ABC) to reduce margin for breathing motion. *Int J Radiat Oncol Biol Phys* 1999;44:911–919.
14. Zhang T, Jeraj R, Keller H, *et al.* Treatment plan optimization incorporating respiratory motion. *Med Phys* 2004;31:1576–1586.
15. Zhang T, Keller H, Jeraj R, *et al.* Breathing synchronized delivery—A new technique for radiation treatment of the targets with respiratory motion. *Int J Radiat Oncol Biol Phys* 2003;57:S185–S186.
16. Zhang T, Keller H, Jeraj R, *et al.* Lung motion tracking with a combined spirometer-laser sensor system. Presented at the AAPM 44th annual meeting, Montreal, 2002.
17. Zhang T, Keller H, O'Brien MJ, *et al.* Application of the spirometer in respiratory gated radiotherapy. *Med Phys* 2003; 30:3165–3171.
18. Lujan AE, Larsen EW, Balter JM, *et al.* A method for incorporating organ motion due to breathing into 3D dose calculations. *Med Phys* 1999;26:715–720.
19. Shirato H, Shimizu S, Kunieda T, *et al.* Physical aspects of a real-time tumor-tracking system for gated radiotherapy. *Int J Radiat Oncol Biol Phys* 2000;48:1187–1195.
20. Neicu T, Shirato H, Seppenwoolde Y, *et al.* Synchronized moving aperture radiation therapy (SMART): Average tumour trajectory for lung patients. *Phys Med Biol* 2003;48:587–598.
21. Manke D, Nehrke K, Bornert P. Novel prospective respiratory motion correction approach for free-breathing coronary MR angiography using a patient-adapted affine motion model. *Magn Reson Med* 2003;50:122–131.
22. Lu W, Parikh PJ, El Naqa IM, *et al.* Quantitation of the reconstruction quality of a four-dimensional computed tomography process for lung cancer patients. *Med Phys* 2005;32: 890–901.
23. Low DA, Parikh PJ, El Naqa IM, *et al.* Quantitative 4-D CT using a multislice CT scanner. In: Yi BY, Ahn SD, Choi EK, *et al.* editors. Proceedings of the 14th international conference on the use of computers in radiation therapy. Seoul, Korea: Jeong Publishing; 2004. p. 57–61.
24. Lu W, Low DA, Parikh PJ, *et al.* Comparison of spirometry and abdominal height as four dimensional computed tomography metrics in lung. *Med Phys* 2005;32:2351–2357.
25. Weibel ER. Morphometry of the human lung. Berlin: Springer; 1963.
26. Murray JF, Nadel JA. Textbook of respiratory medicine. (3rd ed.). Philadelphia: WB Saunders; 2000.
27. Nystrom MM, Lu W, Parikh P, *et al.* A comparison of spirometry and abdominal height as 4DCT metrics [Abstract]. *Med Phys* 2004;31:1779.
28. Politte DG, Lu W, Whiting BR, *et al.* Improving lung scan temporal resolution using tidal-volume sorted sinograms from 4D CT [Abstract]. *Med Phys* 2004;31:1779.
29. Wahab S, Low DA, El Naqa IM, *et al.* Use of four-dimensional computed tomography in conformal therapy planning for lung cancer [Abstract]. *Med Phys* 2003;30: 1364.
30. Wahab S, Parikh P, Lu W, *et al.* Tumor motion mapping using four dimensional computed tomography [Abstract]. *Med Phys* 2004;31:1717.